APPLICATION OF STEGER–WARMING FLUX VECTOR SPLITTING (FVS) METHOD TO NOZZLE FLOW MODELING

Ahmed N. Al-Motlaq, Ibrahim E. Megahed, and Mohammed B. Habeebullah*

Mechanical Engineering Department
King Abdulaziz University
P.O.Box 9027, Jeddah 21413, Saudi Arabia

الخلاصـة :

تُطـوِّر هذه الدراسة برنامج حاسوبي لمحاكاة سريان دوراني غير لزج داخل منافث ملتمة ومنفرجة، وملتمة منفرجة ثنائية البعد وذلك بحل معادلات أويلر. وقد تَـمَّ ذلك باستخدام طريقة فصل متجهات الدفق المطورَّة بواسطة ستيجر ووارمنج (١٩٨١م). وهذه الطريقة تُـعـدُّ من أحدث طرق الفروق المتناهية أُحادية الاتجاه والتي تعتمد على تتبع المنحى الفيزيائي للسريان وبذلك تكون أقرب للواقع من طرق الفروق المتناهية المتوسطة التي يضاف اليها لزوجة اصطناعية لضمان استقرار الحل وهذا يتنافى مع طبيعة المعادلات الحاكمة للسريان (معادلات أويلر) غير اللَّزجة. وقد تَـمَّ اختبار البرنامج على حالات السريان تحت الصوتي والانتقالي وفوق الصوتي داخل منافث مختلفة وقد كانت النتائج متطابقة مع الحلول المنشورة لهذه الحالات. وقد تَـمَّ في هذه الدراسة عمل تحليل تقريبي إضافي أمكن بموجبه تحقيق توفير يصل إلى ٦٥٪ من وقت الحَلِّ دون تغيير في النتائج المستخلصة بالمقارنة مع الطريقة المستخدمة والمنشورة. كما تَـمَّ عمل دراسة مقارنة بين طريقة فصل متجهات الدفق وطريقة ماكورميك كإحدى طرق الفروق المتوسطة الشهيرة .

ABSTRACT

The Steger–Warming flux vector splitting is used for the solution of two-dimensional Euler equations. An implicit finite difference scheme is used. A computer code is developed and tested for subsonic, transonic, and supersonic flow regimes. The method is then applied to the flow through a convergent–divergent nozzle and a divergent nozzle, both with strong shocks. Further factorization has been done to the formulated finite difference equations. As a result of the new factorization, the CPU time to reach the steady state solution decreased significantly to about 65% without altering the accuracy. Comprehensive comparisons with the MacCormack method are presented.

*To whom correspondence should be addressed.

APPLICATION OF STEGER–WARMING FLUX VECTOR SPLITTING (FVS) METHOD TO NOZZLE FLOW MODELING

1. INTRODUCTION

Nozzles have wide range of applications in propulsion and aerodynamics and a knowledge of their flow field is important for their design. The steady state solutions of the nozzle flow, which is governed by the Euler equations, are calculated as asymptotic solutions in time.

Many numerical schemes, implicit and explicit, have been developed to solve the unsteady Euler equations in their conservative and non-conservative forms. Accuracy, shock capturing ability, and low computational cost are the three competing goals in the numerical solution of these equations. Explicit schemes are easy to code, but their stability is relatively poor due to the low CFL number, which leads to a large number of iterations and long computing time. Implicit schemes can be used with high CFL numbers, but require, long and complex coding.

Numerical schemes can be classified according to their ability to produce dissipation [1]. Artificial viscosity can be added to the scheme in order to make it dissipative, but this is violating the nature of the Euler equations (inviscid). Some schemes are naturally dissipative because they follow the physical characteristics of the equations [2]. The MacCormack [3] and Steger–Warming FVS methods [4] respectively represent these two types of schemes.

The objective of the present work is to develop a computer code to solve the governing equations for two-dimensional nozzle flows by an implicit version of the Steger–Warming FVS method. The code will be validated by two-dimensional nozzle flow solutions (exact and numerical). Further factorization will be implemented for the formulated finite difference equations. The effect of this further factorization on the solution speed and accuracy will be investigated. Also, a comparative study with the MacCormack method will be conducted.

2. GOVERNING EQUATIONS

The unsteady Euler equations for two dimensional planar/axisymmetric flow can be written in conservative form as:

$$\frac{\partial Q}{\partial t} + \frac{\partial E}{\partial x} + \frac{\partial F}{\partial y} + \alpha H = 0 \tag{2.1}$$

where

$$Q = \begin{pmatrix} \rho \\ \rho u \\ \rho v \\ \rho e_t \end{pmatrix}, \quad E = \begin{pmatrix} \rho u \\ \rho u^2 + p \\ \rho uv \\ (\rho e_t + p)u \end{pmatrix}, \quad F = \begin{pmatrix} \rho v \\ \rho uv \\ \rho v^2 + p \\ (\rho e_t + p)v \end{pmatrix}, \quad H = \frac{1}{y}\begin{pmatrix} \rho v \\ \rho vu \\ \rho v^2 \\ (\rho e_t + p)v \end{pmatrix}$$

and $\alpha = 0$ for planar flow, $\alpha = 1$ for axisymmetric flow.

The above equations can be transformed from physical domain (x,y,t) to computational domain (ξ, η, τ). For a fixed computational domain the governing equations written as follows:

$$\frac{\partial \overline{Q}}{\partial \tau} + \frac{\partial \overline{E}}{\partial \xi} + \frac{\partial \overline{F}}{\partial \eta} + \alpha \overline{H} = 0 \tag{2.2}$$

where $\overline{Q} = \frac{Q}{J}$, $\overline{E} = \frac{1}{J}(\xi_x E + \xi_y F)$, $\overline{F} = \frac{1}{J}(\eta_x E + \eta_y F)$, and $\overline{H} = \frac{H}{J}$.

The non-conservative form will be:

$$\frac{\partial \overline{Q}}{\partial \tau} + A\frac{\partial \overline{Q}}{\partial \xi} + B\frac{\partial \overline{Q}}{\partial \eta} + \alpha \overline{H} = 0, \tag{2.3}$$

where A, B are the jacobians of the equations given by $\frac{\partial \overline{E}}{\partial \overline{Q}}$ and $\frac{\partial \overline{F}}{\partial \overline{Q}}$ respectively [3].

3. NUMERICAL ALGORITHMS

3.1. MacCormack Explicit Formulation

A predictor/corrector scheme with first order accuracy in time and second order accuracy in space applied to the conservation form of Euler equations.

For the first level (predictor) forward differencing is used to provide:

$$\overline{Q}^{*}_{i,j} = \overline{Q}^{n}_{i,j} - \frac{\Delta\tau}{\Delta\xi}\left[\overline{E}^{n}_{i+1,j} - \overline{E}^{n}_{i,j}\right] - \frac{\Delta\tau}{\Delta\eta}\left[\overline{F}^{n}_{i,j+1} - \overline{F}^{n}_{i,j}\right] - \Delta\tau\alpha\overline{H}^{n}_{i,j}\ ; \tag{3.1.1}$$

and for the second level (corrector) backward differencing is used to result in:

$$\overline{Q}^{n+1}_{i,j} = 0.5\left\{\overline{Q}^{n}_{i,j} + \overline{Q}^{*}_{i,j} - \frac{\Delta\tau}{\Delta\eta}\left[\overline{E}^{*}_{i,j} - \overline{E}^{*}_{i-1,j}\right] - \frac{\Delta\tau}{\Delta\eta}\left[\overline{F}^{*}_{i,j} - \overline{F}^{*}_{i,j-1}\right] - \Delta\tau\alpha\overline{H}^{*}_{i,j}\right\} \tag{3.1.2}$$

Artificial viscosity can be added to the scheme in the form of curve smoothing [5, 6]:

$$\overline{Q}_{i,j} = \left[\Phi\,\overline{Q}_{i,j} + \overline{Q}_{i+1,j} + \overline{Q}_{i-1,j} + \overline{Q}_{i,j+1} + \overline{Q}_{i,j-1}\right]/[\Phi + 4]\ , \tag{3.1.3}$$

where Φ is the smoothing factor given by:

$$\Phi \geq \max\left[\frac{1}{\Delta\xi}, \frac{1}{\Delta\eta}\right].$$

3.2. Steger–Warming FVS Formulation

The flux vectors $\overline{E}, \overline{F}$ are homogeneous of degree one in $\overline{Q}$

i.e. $\overline{E}(\alpha\overline{Q}) = \alpha\overline{E}(\overline{Q})$ for any value of α

and $\overline{E} = A\overline{Q}$ where $A = \dfrac{\partial\overline{E}}{\partial\overline{Q}} = X_A\, D_A\, X_A^{-1}$

therefore, $E = X_A\, D_A\, X_A^{-1}\overline{Q}$

The eigenvalues can be split into non-negative and non-positive eigenvalues such that:

$$D_A = D_A^{+} + D_A^{-}\ ;$$

therefore the flux vector can be split as follows:

$$\overline{E} = X_A\,(D_A^{+} + D_A^{-})X_A^{-1}\overline{Q} = \overline{E}^{+} + \overline{E}^{-}$$

and $A^{+} = X_A\, D_A^{+} X_A^{-1}$, $A^{-} = X_A\, D_A^{-} X_A^{-1}$,

where $A^{+} + A^{-} = A$.

The negative part of the flux vector contains terms that travel upstream while positive part terms travel down stream. By replacing $\overline{E}, A$ with $\overline{F}, B$ respectively in the above steps the $\overline{F}$ flux vector can be obtained.

After linearization [3] the governing equations in non-conservative form can be written as follows:

$$\left[I + \Delta\tau\frac{\partial A^{n}}{\partial\xi}\right]\left[I + \Delta\tau\frac{\partial B^{n}}{\partial\eta} + \alpha\Delta\tau C^{n}\right]\Delta\overline{Q} = -\Delta\tau\left[\frac{\partial\overline{E}^{n}}{\partial\xi} + \frac{\partial\overline{F}^{n}}{\partial\eta} + \alpha\overline{H}^{n}\right]. \tag{3.2.1}$$

After flux splitting the above equation can be written as follows:

$$\left\{I + \Delta\tau\left[\frac{\partial}{\partial\xi}(A^+ + A^-)\right]\right\}\left\{I + \Delta\tau\left[\frac{\partial}{\partial\eta}(B^+ + B^-)\right] + \alpha\Delta\tau C\right\}^n \Delta\bar{Q} =$$

$$-\Delta\tau\left\{\frac{\partial}{\partial\xi}(\bar{E}^+ + \bar{E}^-) + \frac{\partial}{\partial\eta}(\bar{F}^+ + \bar{F}^-) + \alpha\bar{H}\right\}^n . \tag{3.2.2}$$

A first order backward difference approximation is used for positive terms and a first order forward difference is used for negative terms in the above equations, which can be solved in two stages obtained by factorization; each stage is a system of block tridiagonal equations. Full descriptions of this factorization are given in [3].

In this study, further factorization has been done to obtain four systems of block bidiagonal equations which are easy to solve. This kind of factorization is mentioned in [5] and recommended for the multispace problems. The four stages are given as follows:

$$\left(I + \frac{\Delta\tau}{\Delta\xi}A^+_{i,j}\right)\Delta\bar{Q}^{***}_{i,j} + \left(-\frac{\Delta\tau}{\Delta\xi}A^+_{i-1,j}\right)\Delta\bar{Q}^{***}_{i-1,j} = RHS \tag{3.2.3}$$

$$\left(I - \frac{\Delta\tau}{\Delta\xi}A^-_{i,j}\right)\Delta\bar{Q}^{**}_{i,j} + \left(\frac{\Delta\tau}{\Delta\xi}A^-_{i-1,j}\right)\Delta\bar{Q}^{**}_{i+1,j} = \Delta\bar{Q}^{***}_{i,j} \tag{3.2.4}$$

$$\left(I + \frac{\Delta\tau}{\Delta\eta}B^+_{i,j}\right)\Delta\bar{Q}^{*}_{i,j} + \left(-\frac{\Delta\tau}{\Delta\eta}B^+_{i-1,j}\right)\Delta\bar{Q}^{*}_{i,j-1} = \Delta\bar{Q}^{**}_{i,j} \tag{3.2.5}$$

$$\left(I - \frac{\Delta\tau}{\Delta\eta}B^-_{i,j} + \alpha\Delta\tau C_{i,j}\right)\Delta\bar{Q}_{i,j} + \left(\frac{\Delta\tau}{\Delta\eta}B^-_{i,j+1}\right)\Delta\bar{Q}_{i,j+1} = \Delta\bar{Q}^{*}_{i,j} \tag{3.2.6}$$

where

$$RHS = -\Delta\tau\left[\frac{1}{\Delta\xi}\left(\bar{E}^+_{i,j} - \bar{E}^+_{i-1,j} + \bar{E}^-_{i+1,j} - \bar{E}^-_{i,j}\right) + \frac{1}{\Delta\eta}\left(\bar{F}^+_{i,j} - \bar{F}^+_{i,j-1} + \bar{F}^-_{i,j+1} - \bar{F}^-_{i,j}\right) + \alpha\bar{H}_{i,j}\right].$$

4. NUMERICAL RESULTS

4.1. Code Validation

The code is tested by three different nozzles for different flow regimes.The first case is radial flow in a subsonic nozzle with an angle of convergence equal to 45° [7] given in Figure 1. The results obtained are shown in Figures 2 and 3: they are identical to the exact solution within a maximum percentage error in the computed Mach number of 1.36%, compared with the exact value. The second case is transonic flow in a convergent divergent nozzle with strong shock given in [5]. Figure 4 shows good agreement with the recent technique. The shock has been captured 5% of the nozzle length downstream from the position of the reference technique used in [5]. This slight deviation in shock position is a result of the solution technique. The reference technique is based on some approximations that could affect the solution accuracy. Artificial viscosity which is added to maintain stability violates the nature of the Euler equations (inviscid) while the amount of the added viscosity will affect the shock position and shape. The second approximation in the reference method is due to the assumption of constant enthalpy all over the nozzle field and excludes the energy equation (only continuity and momentum equations are solved). Consequently, the FVS method which has no such approximations is more accurate than the reference method. The third case is a full supersonic convergent divergent duct with 4% thick circular arc bump given in [8]. The results are shown in Figure 5. The two solutions are almost identical.

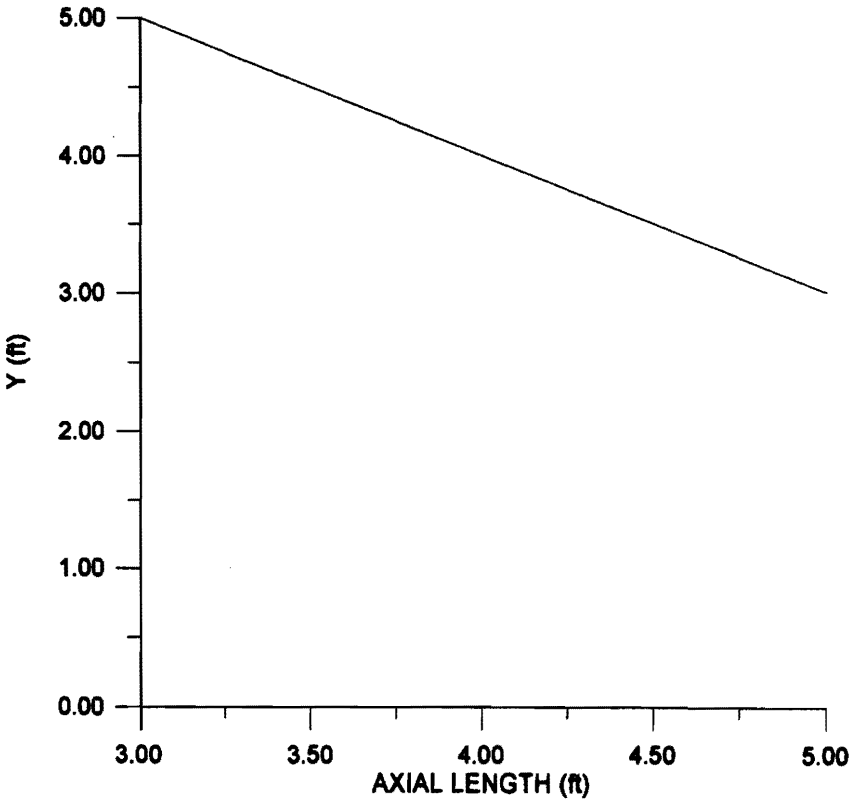

Figure 1. Convergent Nozzle Geometry.

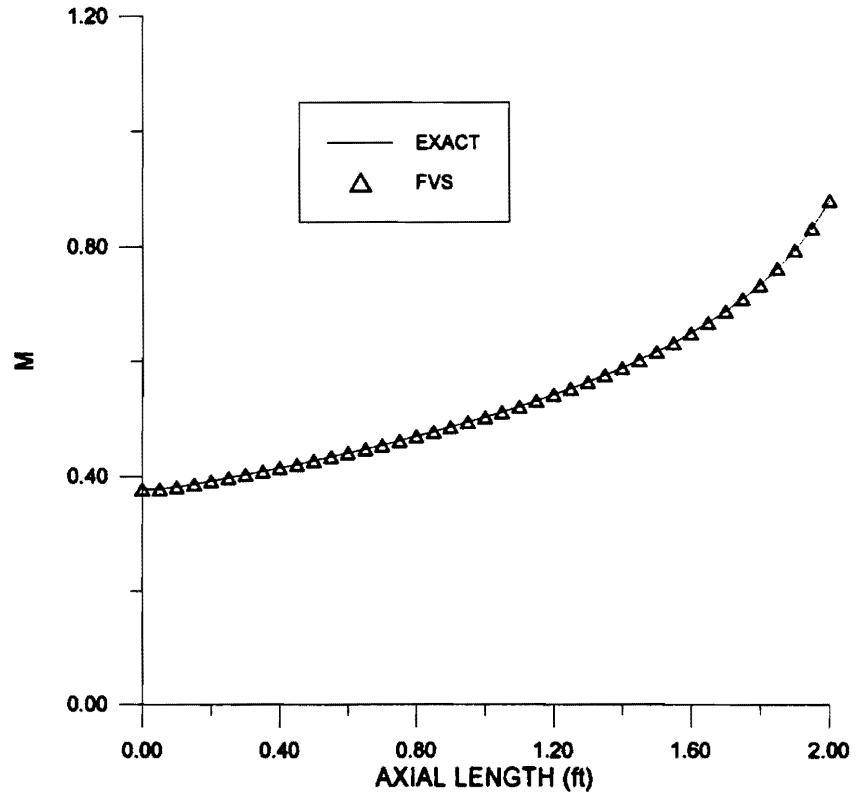

Figure 2. Comparison Between the Exact and Numerical Solutions of the Convergent Nozzle Flow.

4.2. Applications

After validation, the code for the FVS method and another code developed for MacCormack method were applied for two different nozzles in order to compare the two techniques. Further factorization, as discussed before, will be investigated.

4.2.1. Nozzle Geometry

(I) Axisymmetric convergent divergent nozzle with wall contour given by

$$r(x) = 1 + 0.05x^2 \qquad -2 \le x \le 2$$

(II) Planar divergent nozzle with wall contour given by

$$y_w = 1 + 0.27x \qquad 0 \le x \le 3.$$

The shapes of the two nozzles are shown in Figure 6.

4.2.2. Solution Grids

For the first nozzle, a uniform H-grid with 121×21 points in ξ, η directions respectively was used, while O-grid with 41×17 points was used for the second nozzle. The two grids are shown in Figure 7.

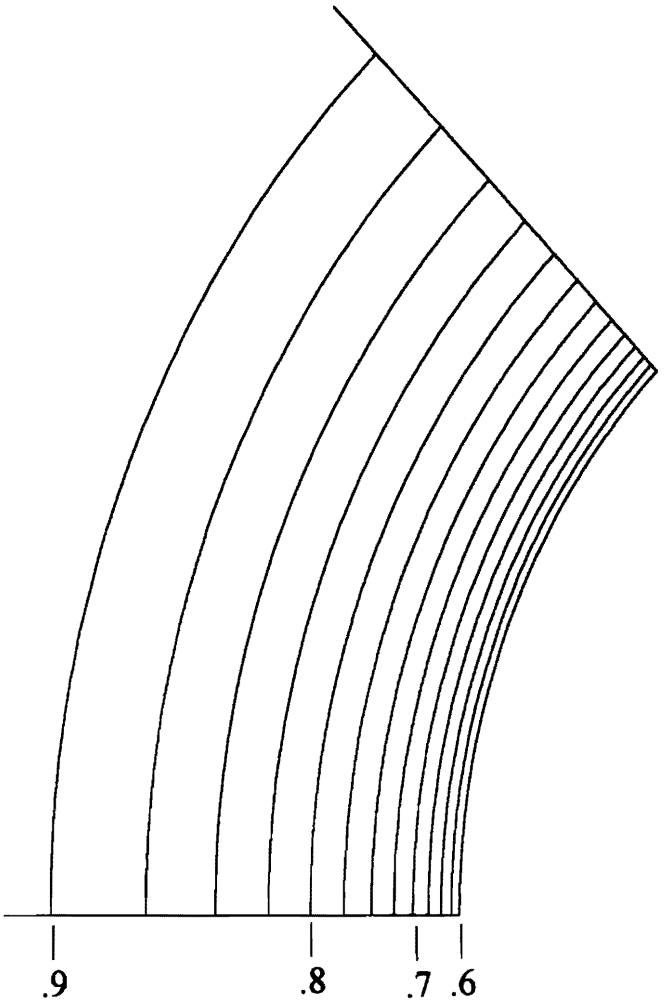

Figure 3. Isobar Lines for Subsonic Nozzle.

4.2.3. Initial and Boundary Conditions

1. Convergent–divergent nozzle

   Initially the flow is at rest (zero velocity) with total pressure and total temperature all over the field. The solution is started by imposing the static pressure value at the exit to capture the shock in the divergent section. At the inlet, total temperature and total pressure are fixed while the velocity components are updated from the interior by two points extrapolation. The other flow variables can be calculated. At the exit, the static pressure is imposed, while density and velocity components are extrapolated from the interior.

2. Divergent nozzle

   Initially the flow is supersonic all over the nozzle with Mach number equals to the inlet Mach number of 1.13. At the inlet the flow is supersonic and therefore all the eigenvalues are positive which requires three analytical boundary condition to be imposed at the inlet (pressure, density, and velocity). The other flow variables can be calculated. In order to capture the shock in the nozzle, the exit boundary conditions are the same as for the first nozzle. For fully supersonic flow, the flow variables are extrapolated from the interior and there is no need to impose any of them at the exit.

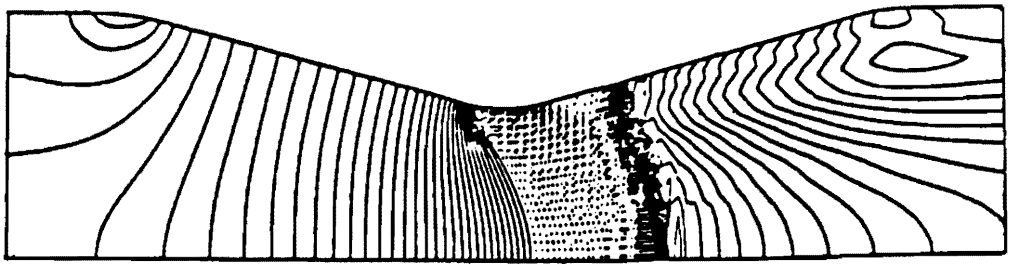

a. Explicit central scheme ref. [5].

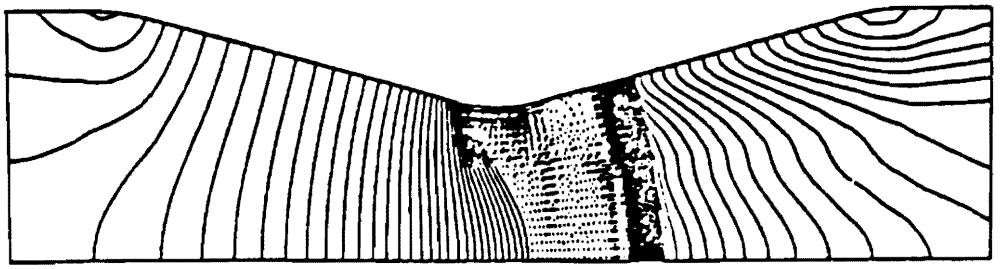

b. Implicit central scheme ref. [5].

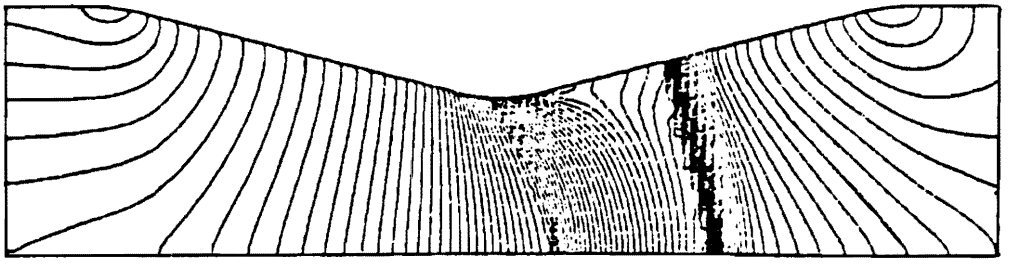

c. Implicit FVS.

Figure 4. Isomach Lines for Convergent–Divergent Nozzle($\Delta M = 0.02$).

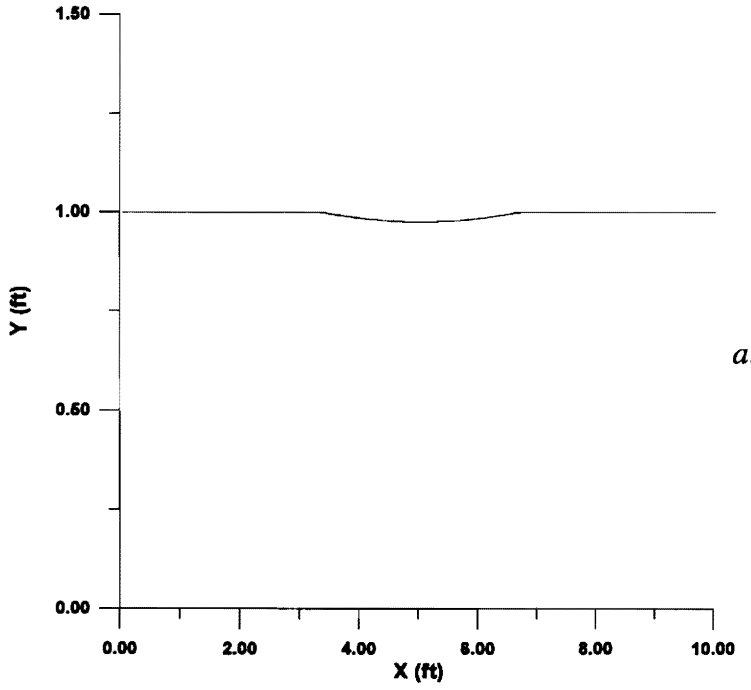

a. Duct geometry.

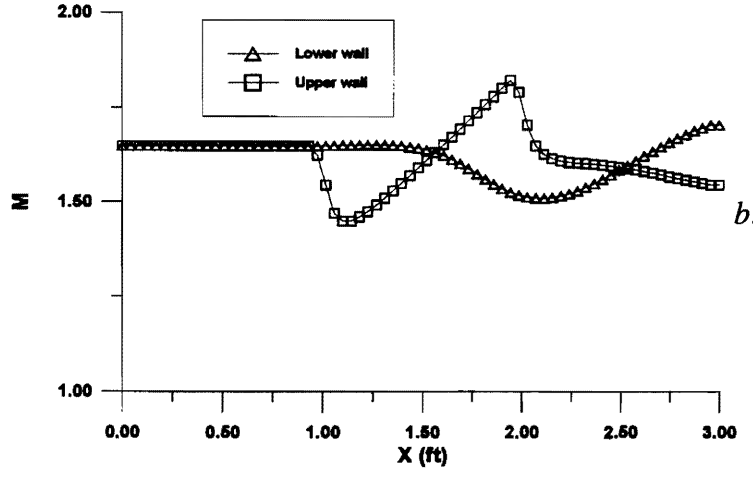

b. Implicit FVS method.

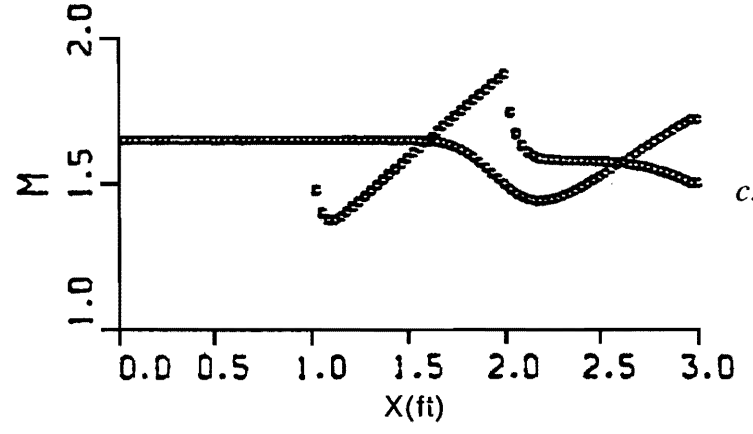

c. Godunov method ref. [8].

Figure 5. Mach Distribution for 4% Thick Circular Arc Bump in the Upper and Lower Walls.

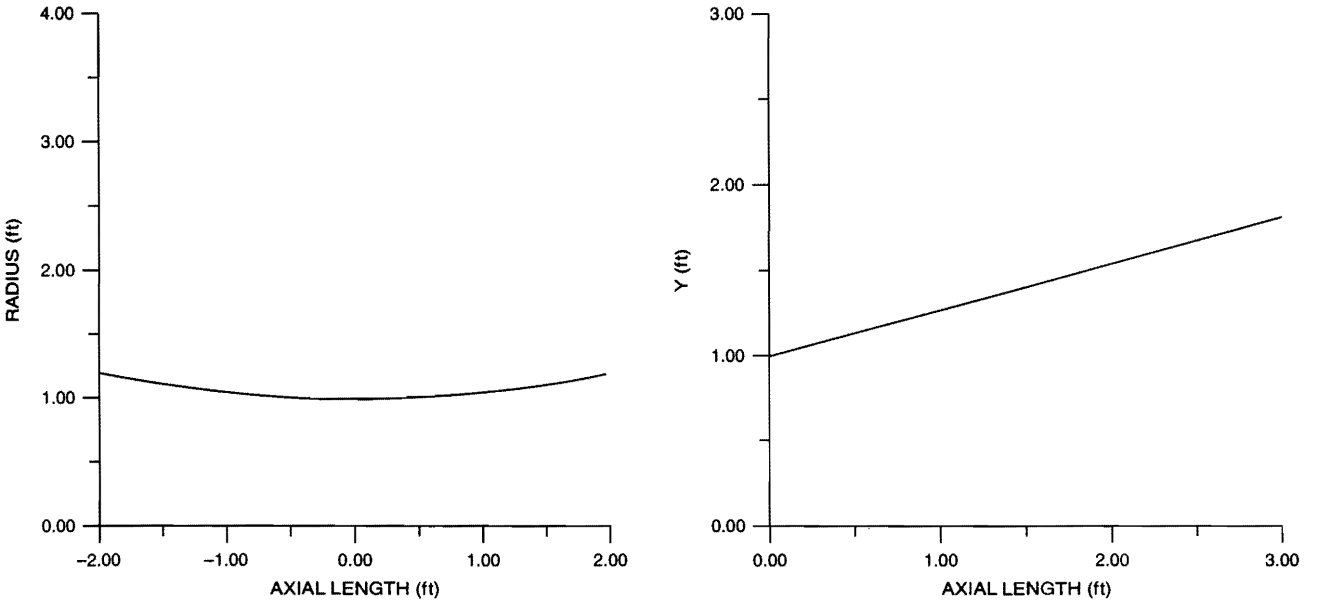

a. convergent–divergent nozzle.

b. divergent nozzle.

Figure 6. The Geometries of the Convergent Divergent and Divergent Nozzles.

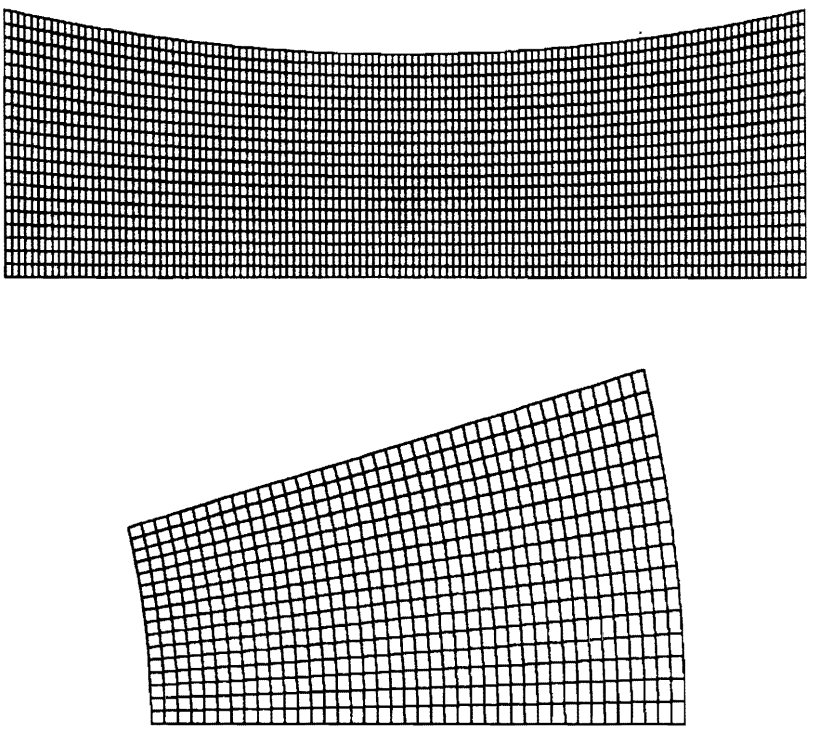

Figure 7. Computational Grids for the Convergent–Divergent and Divergent Nozzles.

For both nozzles, at the axis of symmetry reflection technique is used [9–11]. At the wall, the tangential contravariant velocity U is extrapolated linearly from the interior to ensure the slip condition and the normal contravariant velocity V is zero to ensure no mass flux through the solid boundary. Pressure and density at the wall are extrapolated from the interior. The contravariant velocities U and V are given as follows

$$U = u\xi_x + v\xi_y$$

$$V = u\eta_x + v\eta_y .$$

4.2.4. FVS and MacCormack Method

For the convergent–divergent nozzle, the two methods were run at the same CFL; the steady state solution obtained after almost the same number of iterations while the time per iteration is six times larger in the case of FVS method than with MacCormack method with artificial viscosity ($\Phi = 31$). Generally the results are almost the same; Figures 8, 9 show the Mach number variation along the nozzle axis and upper wall. We can notice, in the case of the FVS method, the glitch in the throat area where some of the eigenvalues are zero at the sonic flow while the algorithm deals with negative and positive eigenvalues (subsonic and supersonic flow) only. It is recommended to add a small positive number (blending term) to the eigenvalues so they will not become zero. Also, at the axis of symmetry the shock is smeared over six grid points more in the case of the MacCormack method than for the FVS method, while it is smeared over eight points at the wall. Figures 10, 11 show the variation of the pressure at the axis of symmetry and the upper wall; little difference can be noticed at the shock.

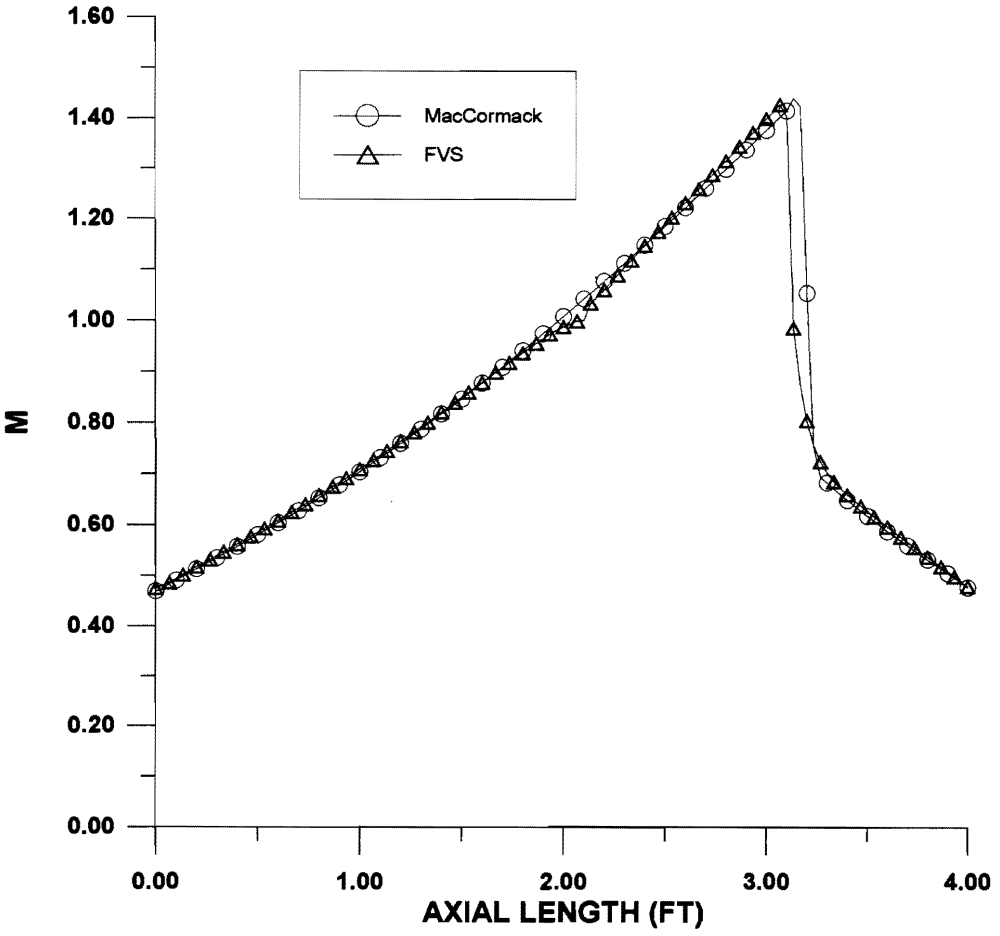

Figure 8. Mach Distribution along the Axis of the Convergent–Divergent Nozzle.

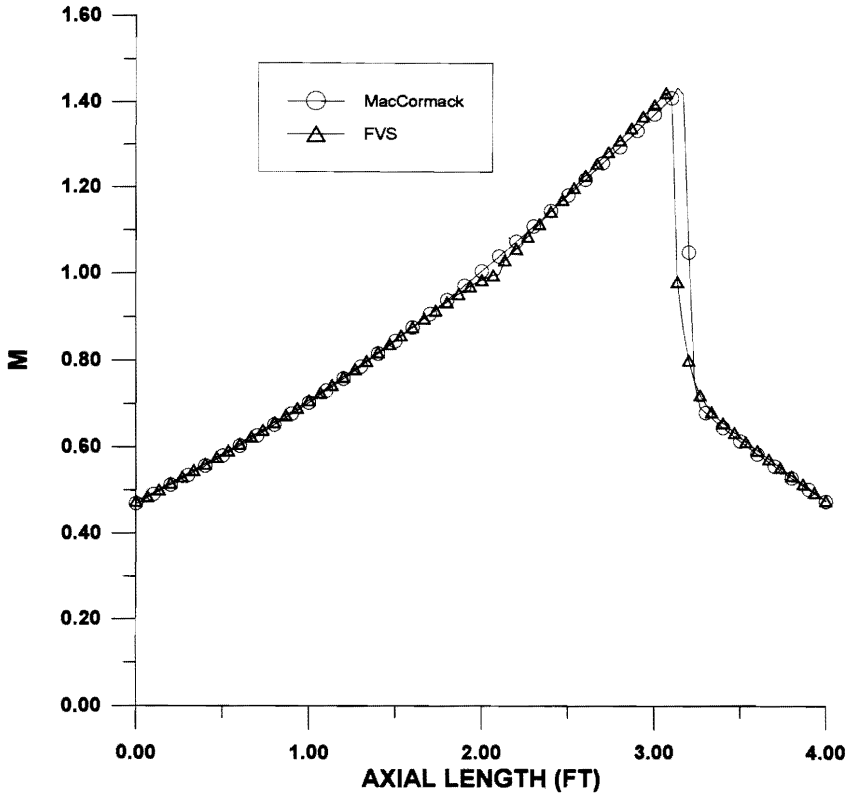

Figure 9. Mach Distribution along the Wall of the Convergent–Divergent Nozzle.

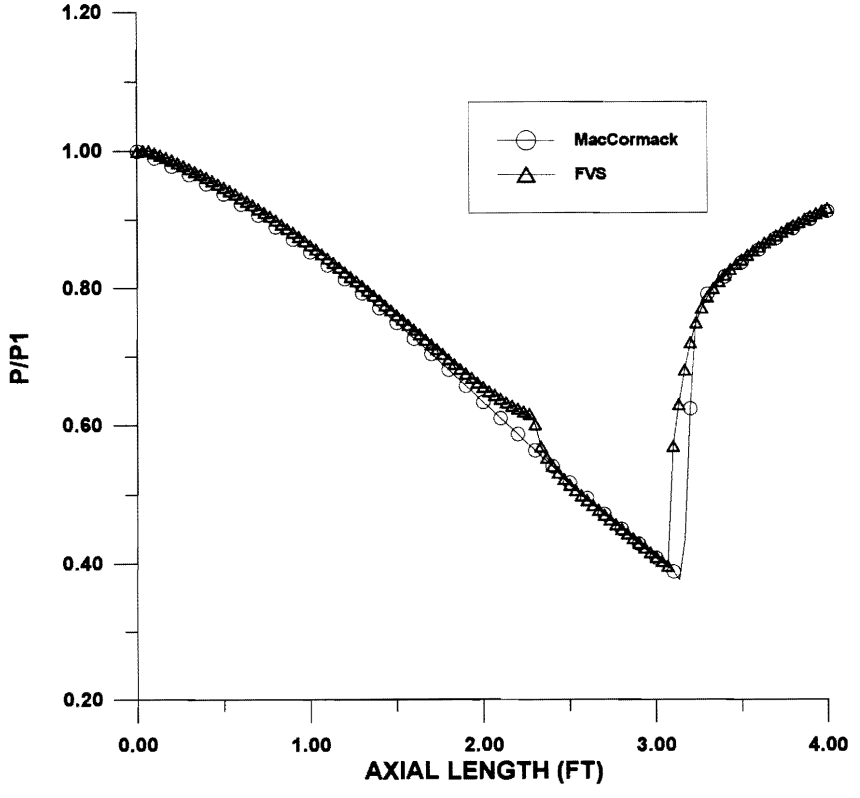

Figure 10. Pressure Distribution along the Axis of the Convergent–Divergent Nozzle.

For the divergent nozzle, Figures 12, 13 show the variation of the Mach number and the pressure. A slight difference between the two methods can be noticed at the supersonic region, with no change in the subsonic region; this is due to the large gradient at the supersonic region. The shock in this case has the same behavior as in the first case, *i.e.* smeared over more grid points in the case of the MacCormack method; this can be noticed clearly from Figure 14.

In the case of the convergent–divergent nozzle the maximum CFL number used in the FVS method is two times greater than that for the MacCormack method and the CPU time per iteration is three times greater. While the maximum CFL number in the case of the divergent nozzle with shock is the same in both methods, if the flow is fully supersonic as shown in Figure 15, the maximum CFL number is five times greater in the FVS than for the MacCormack method.

4.2.5. The Effect of Further Factorization

In Section 3.2 two different techniques to solve the finite difference equations based on approximate factorization are presented. To compare the two techniques the divergent nozzle problem is solved by using each method independently with the same O-type grid, CFL, initial conditions, boundary conditions and convergence criterion. The two solutions, as shown in Figure 16, are the same; the steady state solution is obtained after the same number of iterations and the same time of integration. The convergence history is given in Figure 17; where the convergence criterion is given as

$$\varepsilon = \left| \frac{\sum_{i=1}^{im} P^{n}_{i,jm} - \sum_{i=1}^{im} P^{n-1}_{i,jm}}{\Delta t} \right| \leq 10^{-7} .$$

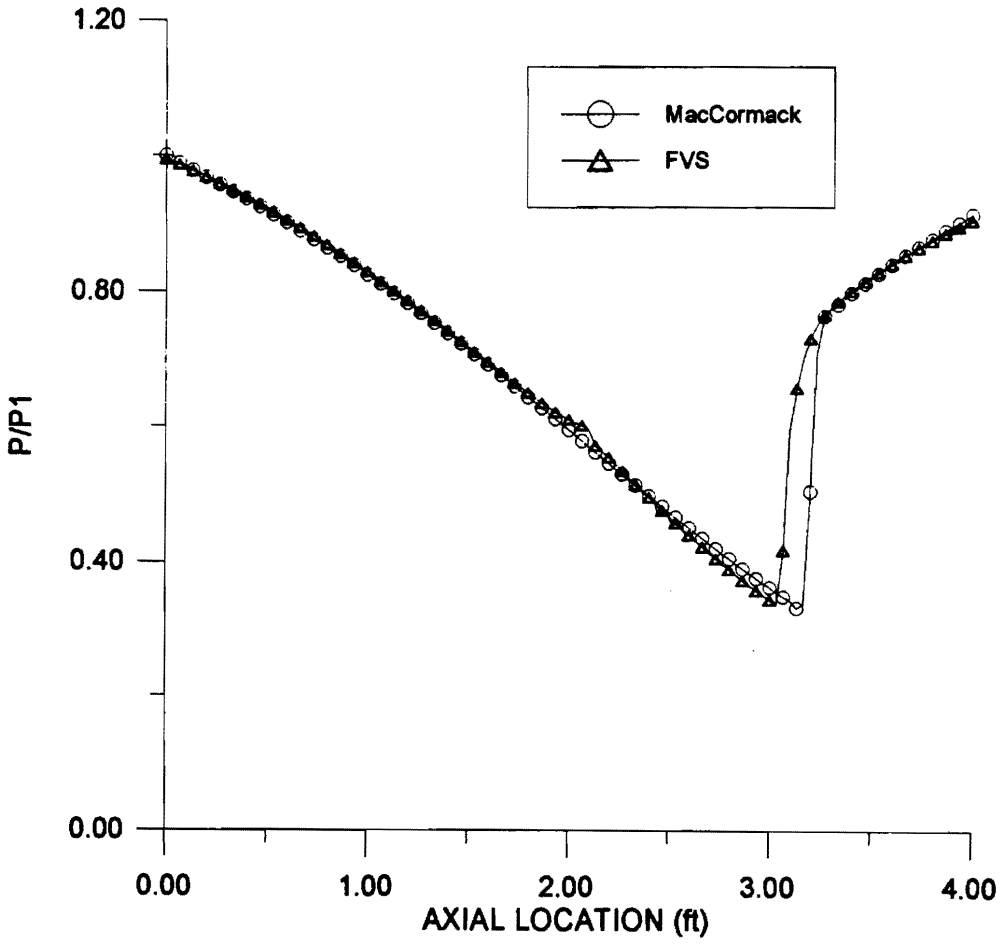

Figure 11. Pressure Distribution along the Wall of the Convergent–Divergent Nozzle.

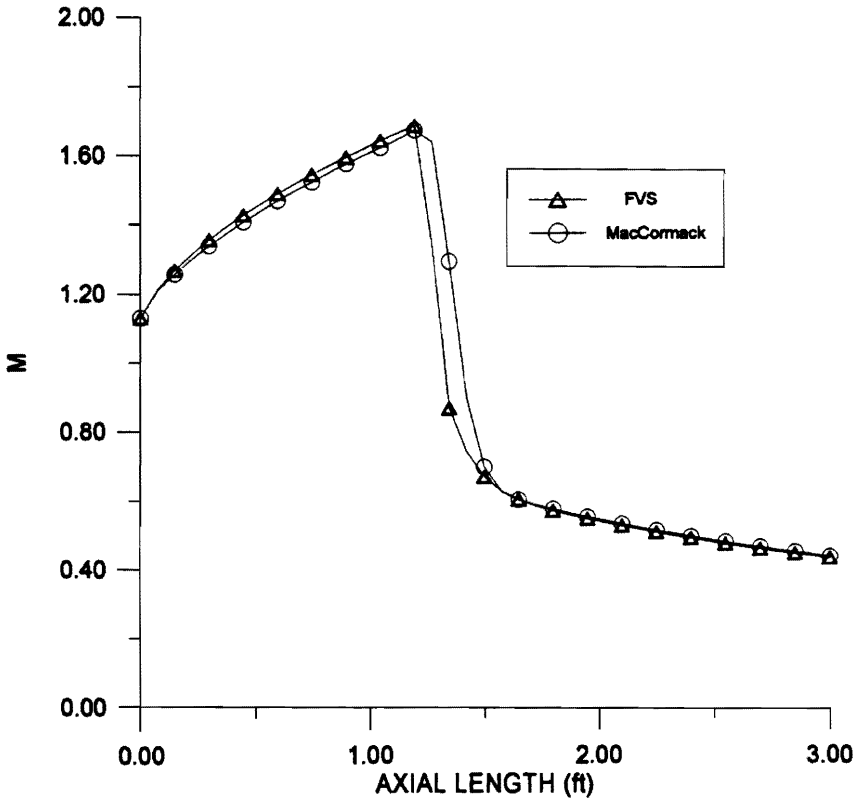

Figure 12. Mach Distribution along the Divergent Nozzle.

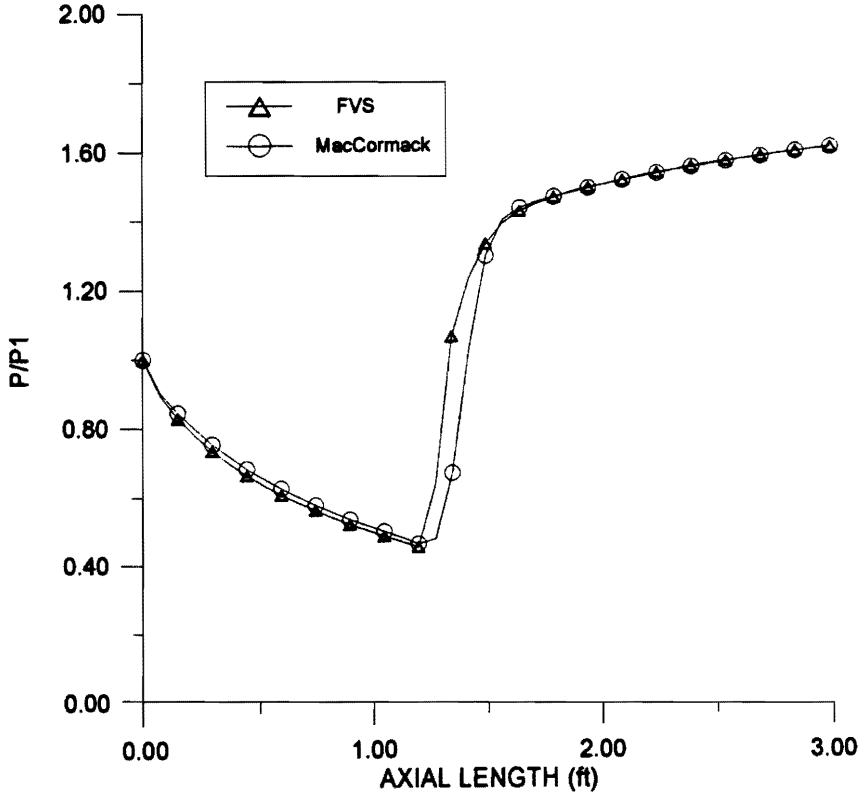

Figure 13. Pressure Distribution along the Divergent Nozzle.

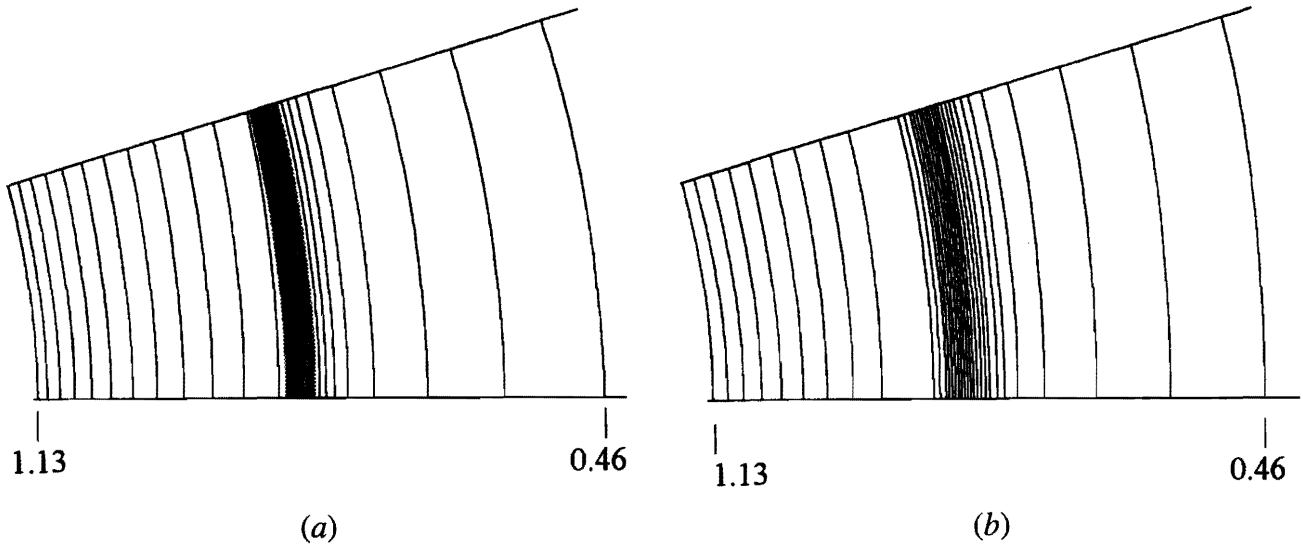

Figure 14. Isomach Lines in the Divergent Nozzle (ΔM = 0.04).
(a) *FVS;* (b) *MacCormack.*

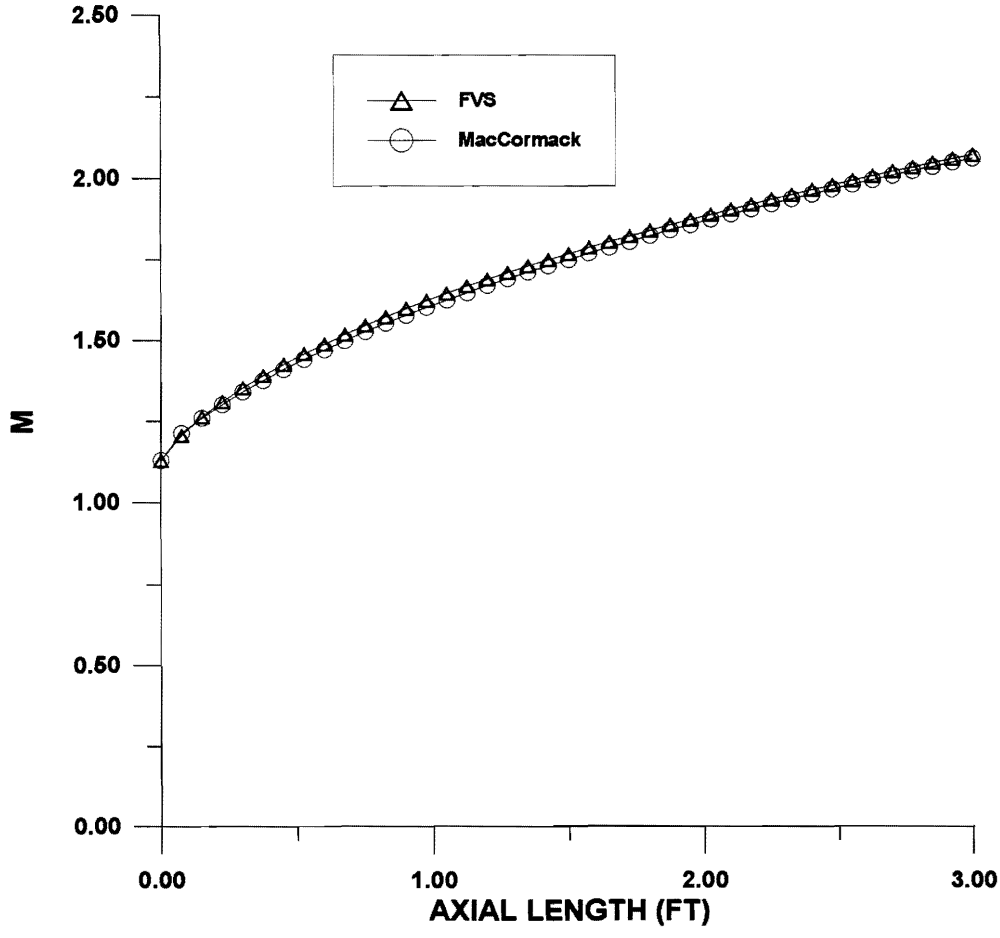

Figure 15. Mach Distribution along the Axis of the Divergent Nozzle.

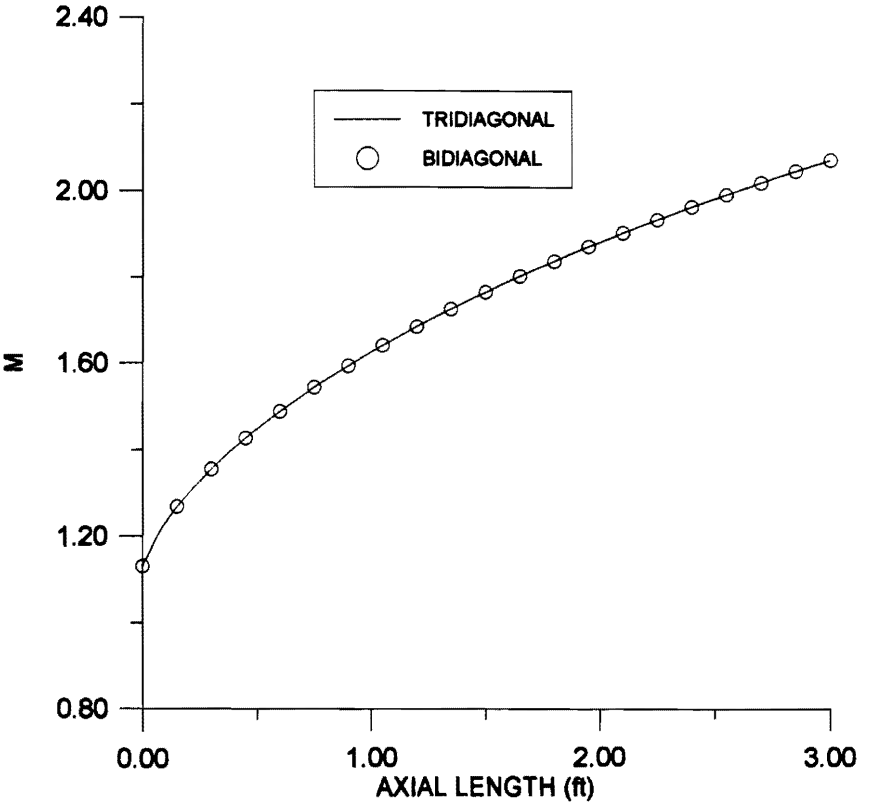

Figure 16. Comparison Between the Two Methods of Factorization.

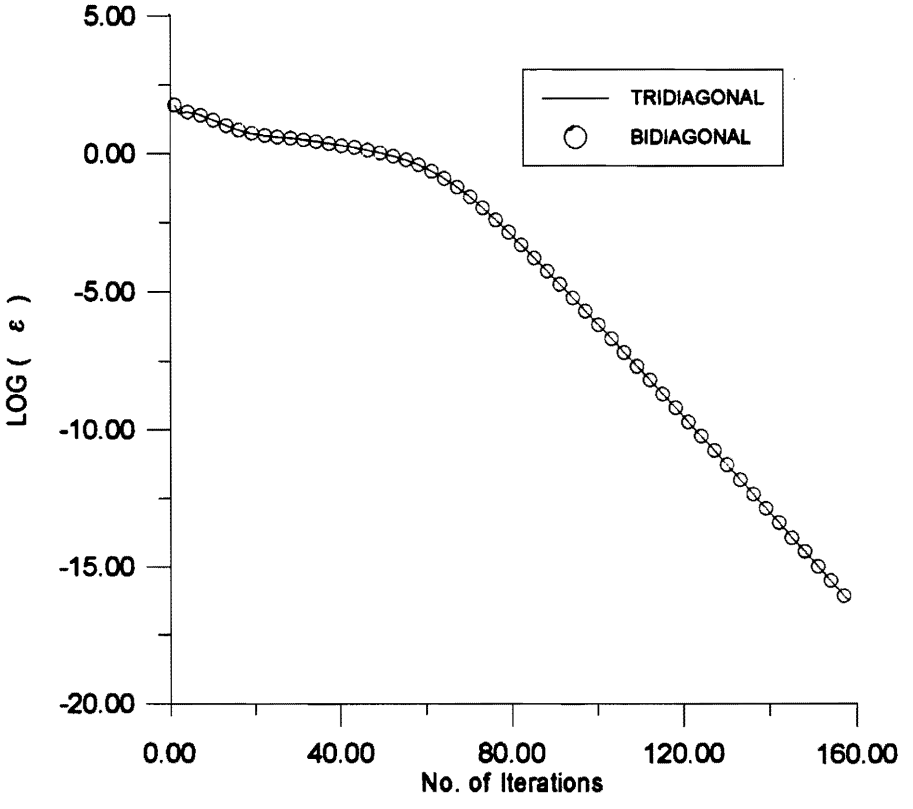

Figure 17. Solution Convergence History.

The CPU time per iteration is reduced significantly for the second technique (block bidiagonal) compared to the first (block tridiagonal). The reduction in CPU time varies from one case to the other; depending on the number of grid points. Table 1 shows the time per iteration for different grids. It can be noticed that the finer the grid, the greater is the reduction rate.

Table 1. Convergence CPU Time Comparison*.

Grid	Time / Iter. Bidiagonal	Time / Iter. Tridiagonal	Reduction Rate
41 × 21	20.6 s	37.35 s	44.8%
61 × 21	30.7 s	56.14 s	45.3%
121 × 21	61.69 s	177.25 s	65.2%

*IBM 486–66 Processor

5. CONCLUSIONS

The FVS and MacCormack methods described in the previous sections have been coded and tested in a variety of flow problems. Both methods gave almost the same results. The FVS method is more accurate; this can be noticed from the crisp shocks and the oscillation free solutions obtained in comparison with the MacCormack method, also from the fact that Euler equations are inviscid while artificial viscosity is added in the MacCormack method. The MacCormack method is easy to code and steady state solution is obtained faster than for the FVS. The maximum CFL number depends on the boundary condition of the flow. In general, the FVS method, due to its implicit formulation, allows a higher CFL number than the MacCormack method in most cases. In addition, artificial viscosity allows a higher CFL number for the MacCormack method than that stated by analytical stability analysis. The major drawback of the FVS method is the large number of calculations, which required more memory and time. This drawback can be overcome by using further factorization, which hugely reduced the CPU time, especially in large grids. In addition, this method has some problems in the sonic region. The glitch that appeared in that region is due to the eigenvalues approaching zero, which could damage the solution. Adding a blending term will prevent the eigenvalues from becoming zero which improves the solution stability. Another error inherited due to the addition of the blending term is that the summation of the split flux vectors (E^+, E^-, F^+, and F^-) will no longer equal the original (non-split) flux vectors E and F. It is recommended to use finer grid at that area which will minimize the glitch influence but will not solve the problem.

NOMENCLATURE

Latin

A	Jacobian matrix of the flux vector $\bar{E}$	
B	Jacobian matrix of the flux vector $\bar{F}$	
C	Jacobian matrix of the flux vector $\bar{H}$	
D	Matrix of eigenvalues	
E	Flux vector in x-direction	
e_t	Total energy	[m^2/s^2]
F	Flux vector in y-direction	
H	Axisymmetry flux vector	
I	Identity matrix	
J	Jacobian of transformation	
p	Pressure	[N/m^2]
Q	Dependent variables vector	
r	Axisymmetric nozzle radius	[m]
t	Time	[s]

u	Velocity component in x-direction	[m/s]
v	Velocity component in y-direction	[m/s]
X	Eigenvector matrix	
x	x-Direction	[m]
y	y-Direction	[m]

Greek

Δ	Increment in time or space	
τ	Time in computationl domain	[s]
ρ	Density	[kg/m^3]
ξ	Curvilinear coordinate direction	
η	Curvilinear coordinate direction	

Subscript

A	Associated with jacobian A
w	Planar nozzle wall

Superscript

+	Associated with positive split vector
–	Associated with negative split vector
n	Time level
*	Intermediate value in multi-step integration level
_	Dimensionless value in computational domain.

REFERENCES

[1] U. Muller, K. Roesner, and B. Schmidt, *Recent Developments in Theoretical and Experimental Fluid Mechanics*. Berlin: Springer-Verlag, 1979, pp. 157–165.

[2] P. L. Roe, "Characteristics-Based Schemes for the Euler Equations", *Annual Review of Fluid Mechanics,* **18** (1986), pp. 337–365.

[3] K. Hoffman and S. Chiang, "Computational Fluid Dynamics for Engineers", in *Engineering Education System,* vols. I and II. Wichita, Kansas: Engineering Education System, 1993.

[4] J. Steger and R. Warming, "Flux Vector Splitting of the Inviscid Gasdynamics Equations with Application to Finite Difference Methods", *J. Computational Physics,* **40** (1981), pp. 263–293.

[5] M. Abdelrahman, "Implicit Pseudo-Unsteady Method for Solving Euler Equations in Transonic Flow", *La Recherche Aerospatiale,* **2** (1983), pp. 87–93.

[6] X. Zhou and S. Liu, *Flow Phenomena and Measurements.* Houston, Texas: Gulf Publishing Company, 1986.

[7] T. Fransson, "Application of Flux Vector Splitting Methodology Towards the Solution of Unsteady Transonic Flow", *Final Report NPS 67-87-006, Naval Postgraduate School, Monterey, CA*, 1987.

[8] S. Eidelman, P. Colella, and R. Shreeve, "Application of the Godunov Method and Its Second-Order Extension to Cascade Flow Modelling", *AIAA*, November 1984, pp. 1609–1615.

[9] H. Onslow, "Solution Acceleration and Accuracy Improvements for Navier–Stokes Solvers", *Ph.D. Dissertation, University of Illinois at Urbana-Champaign,* 1994.

[10] D. Anderson, J. Tannehill, and R. Pletcher, *Computational Fluid Mechanics and Heat Transfer*. New York: Hemisphere Publishing Corporation, 1984.

[11] A. N. Al-Motlaq, "Numerical Solution of Euler Equations for Unsteady Two Dimensional Nozzle Flow Using Flux Vector Splitting Method", *Masters Thesis, King Abdulaziz University, Jeddah, K.S.A.*, 1996.

Paper Received 6 February 1996; Revised 13 July 1996; Accepted 31 December 1996.